Electronic Supplementary Material (ESI) for Nanoscale.

Supporting Information

Ion Transport Based Structural Description for *in situ* Synthesized SBA-15 Nanochannels in a Sub-micropipette

Rui Zhang[a], Qiang Zeng[*a], Xuye Liu[b], and Lishi Wang[*a]

[a]School of Chemistry and Chemical Engineering, South China University of Technology, Guangzhou, China

[b]Shantou Institute for Inspection, Shantou , China

Corresponding Authors

E-mail: ceqzeng@scut.edu.cn; wanglsh@scut.edu.cn

Table of Contents

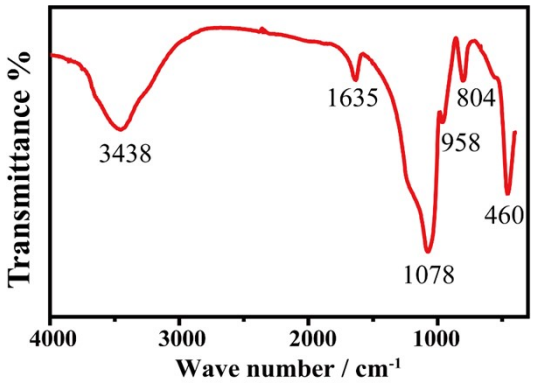

Figure S1. FT-IR spectra of SBA-15 powder. The peaks at 460, 804, and 1078 cm^{-1} correspond to the formation of condensed siloxane networks, the weak peak around 958 cm^{-1} comes from the bending vibration of non-condensed Si-OH. The small peak at 1635 cm^{-1} and the broad peak at 3438 cm^{-1} are from the stretching vibrations of the sample adsorbed water molecules and bending vibrations of the O-H bond, respectively.[1] The result shows the successful synthesis of pure silica particles and the complete removal of the organic template.

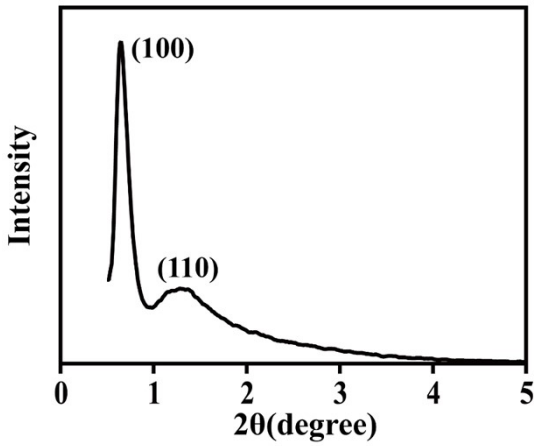

Figure S2. The small-angle XRD pattern of SBA-15 powder. The two diffraction peaks observed correspond to (100) and (110) crystal planes, respectively. It is demostrated that well-resolved hexagonal pore structures are obtained after calcination,[2] and the corresponding pore size is calculated to be 6.82 nm according to the Bragg equation.

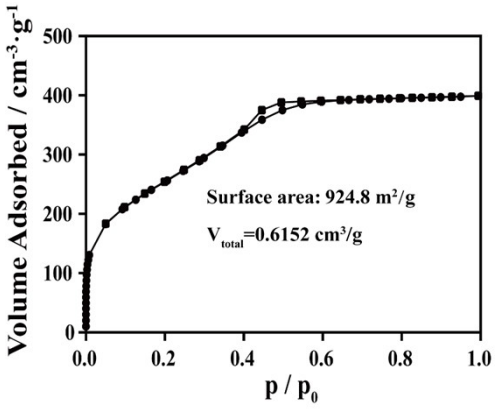

Figure S3. BET of SBA-15 powder. The sample was degassed at 150 °C for 4 h to obtain BET curve. The results show that the BET surface area is 924.8 m^2/g, and the pore volume is 0.6152 cm^3/g, which is consistent with previous report,[3] indicating that SBA-15 features small pore diameter and nanochannel structure.

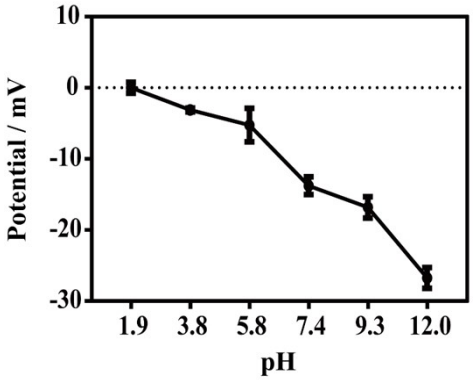

Figure S4. The relationship between ζ-potential of SBA-15 particles and pH. Although the pI of Si-OH is 3, SBA-15 exhibits a ζ-potential close to 0 at pH 1.9, and the negative ζ-potential increase with increasing pH. It is speculate that the mesoscopic organization of SBA-15 exposes a large number of Si-OH, such that an acidity (pH 1.9) slightly above the pI is not sufficient for SBA-15 to exhibit a sufficient positive surface charge.

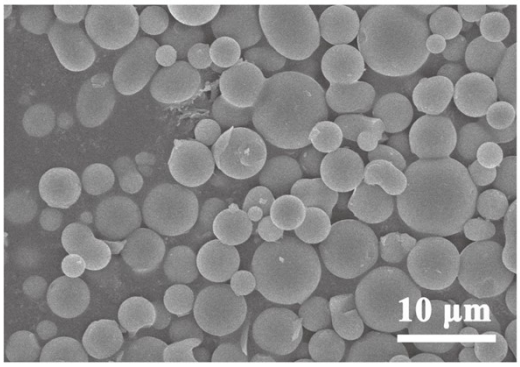

Figure S5. SEM image of SBA-15 powder. The result indicates the successful synthesis of SBA-15 spherical particles in bulk solution.

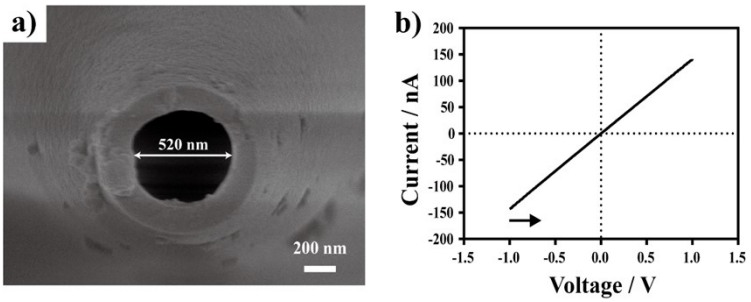

Figure S6. a) SEM image and b) I-V curve in 100 mM KCl solution (pH 7.4, scan rate is 100 mV/s) of 500 nm borosilicate pipette, which bottom is sealed by aqueous and tip is immersed in TEOS. It shows that SBA-15 is not grown at the aperture and the I-V curve reflects an ohmic response, demonstrates removing the air bubbles from the tip is an important part of a successful experiment.

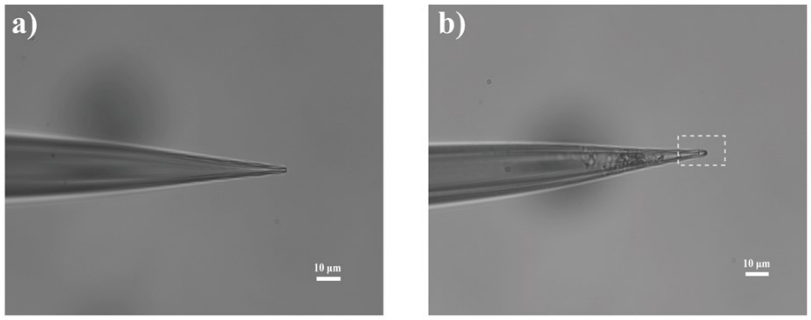

Figure S7. Microscopic photographs of (a) bare sub-mircopipette and (b) GP-SBA-15. SBA-15 is marked by white dotted line, and SBA-15 is a transparent solid.

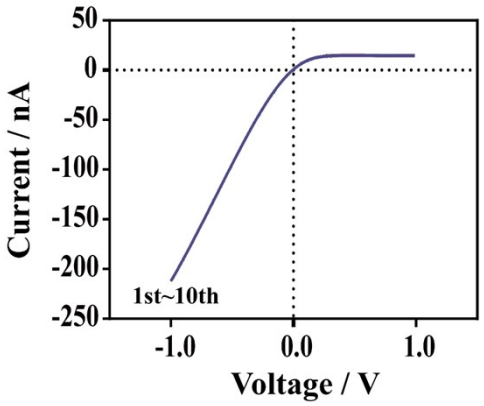

Figure S8. I-V curves of GP-SBA-15 in 100 mM KCl solution (pH 10.0, scan rate is 100 mV/s) for 10 successive measures (the voltage sweep with the direction from -1 V to +1 V), which not only shows that SBA-15 grown *in situ* in a sub-micropipette is stable and does not loosen, but also shows that the accumulation of ions at negative voltages is rapid.

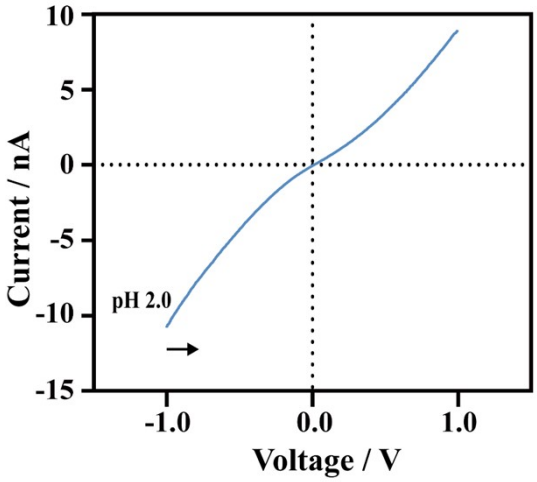

Figure S9. The complete I-V_{-1V} of GP-SBA-15 in 100 mM KCl (pH 2.0, scan rate is 100 mV/s). It is shown that the I-V is almost a straight line, and no rectification is observed.

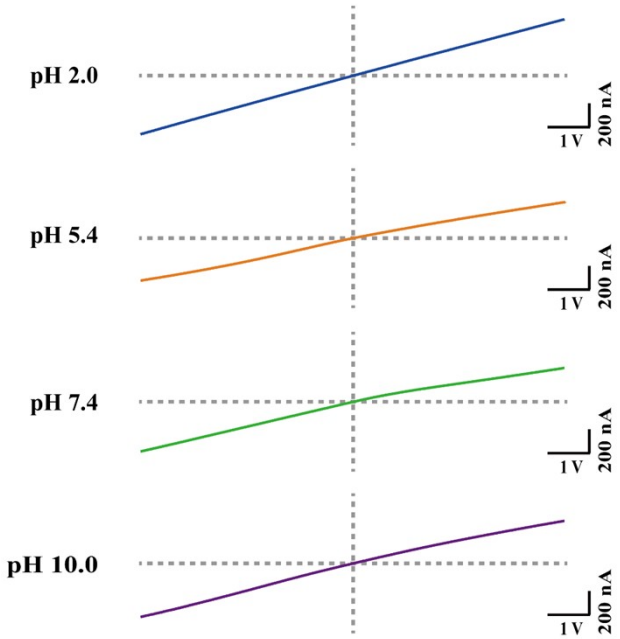

Figure S10. I-V curves of 500 nm bare borosilicate pipettes at different pH from -5 V to +5 V, all I-V curves are recorded in 100 mM KCl and scan rate is 100 mV/s. I-V curves show the ohmic-response.

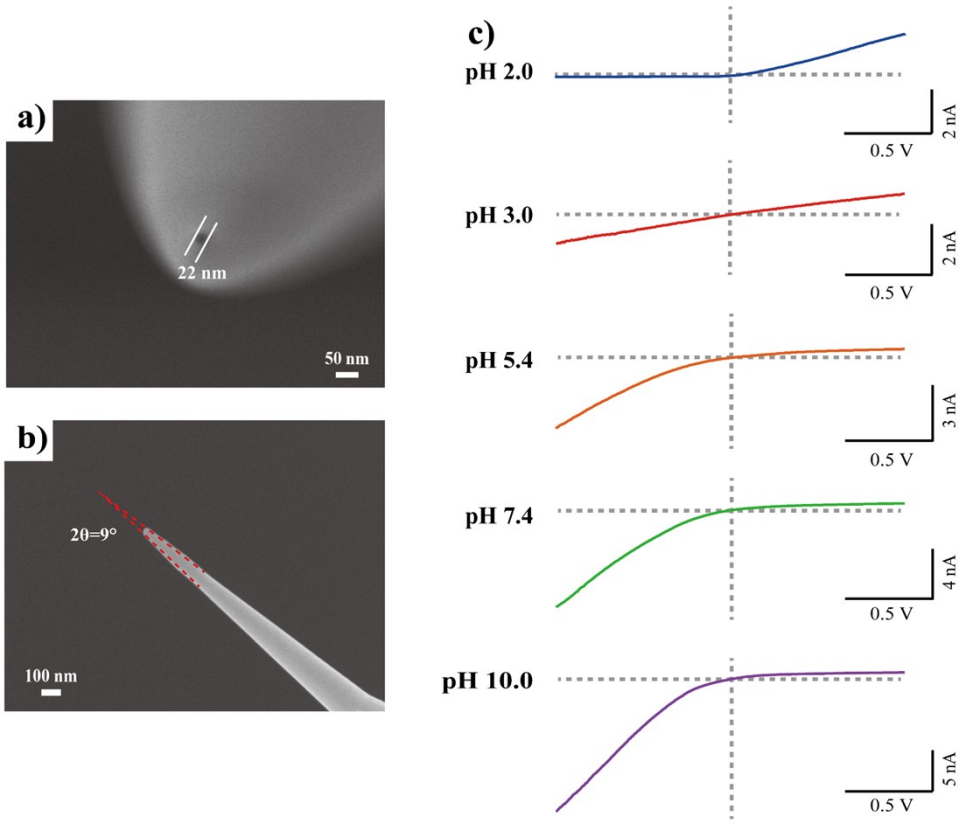

Figure S11. SEM images of 22 nm bare quartz nanopipette: (a) top-view; (b) side-view (2θ=9°). (c) I-V curves of 22 nm nanopipette at diferent pH from -1V to +1V, all I-V curves were recorded in 100 mM KCl and scan rate is 100 mV/s. The results display the pH-dependent ion rectification behavior.

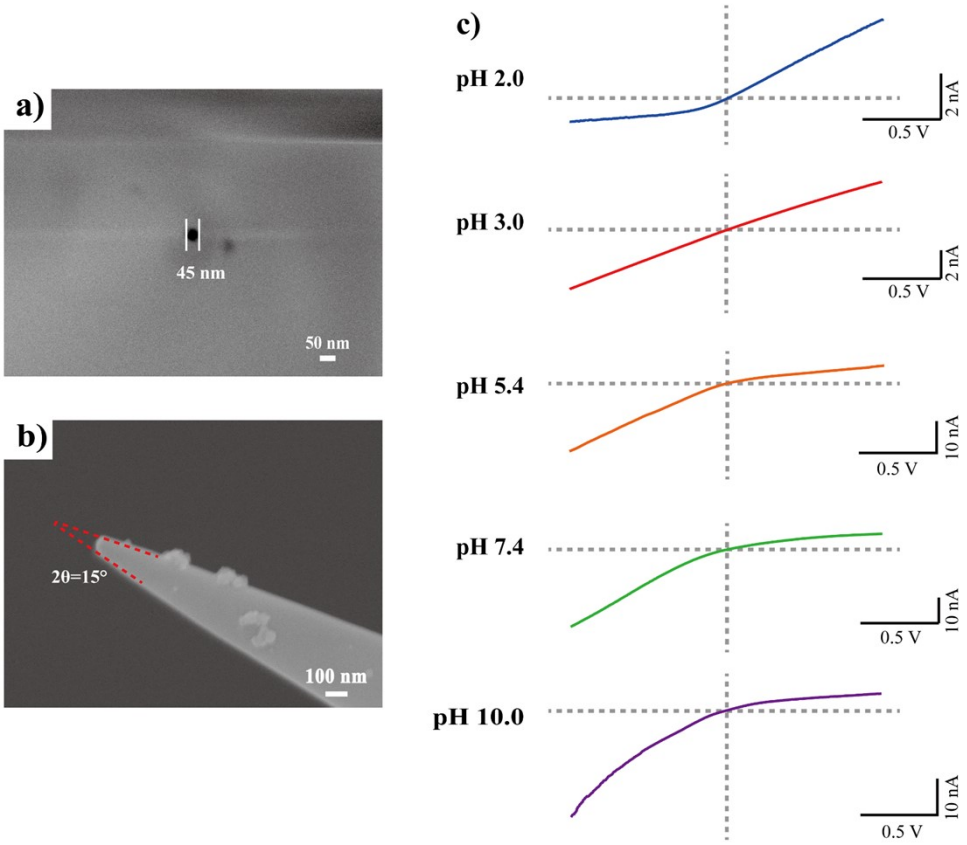

Figure S12. SEM images of 45 nm bare quartz nanopipette: (a) top-view; (b) side-view (2θ=15°). (c) I-V curves of 45 nm nanopipette at diferent pH from -1 V to +1 V, all I-V curves are recorded in 100 mM KCl and scan rate is 100 mV/s. The results also display the pH-dependent ion rectification behavior. In addition, it is clear that the current value of the 45 nm nanopipette is greater than that of 22 nm nanopipette from the Figure S10c and S11c.

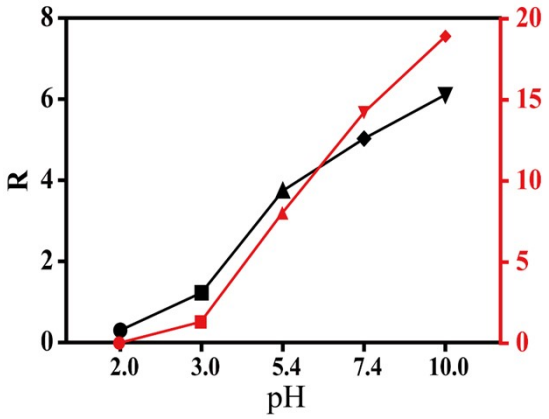

Figure S13. The relationship between the R-value of quartz nanopipette and pH calculated from Figure S11 and S12. Black: 45 nm nanopipette, $R_{2.0}$=0.30, $R_{3.0}$=1.23, $R_{5.4}$=3.75, $R_{7.4}$=5.03, $R_{10.0}$=6.11; red: 22 nm nanopipette, $R_{2.0}$=0.03, $R_{3.0}$=1.32, $R_{5.4}$=8.04, $R_{7.4}$=14.22, $R_{10.0}$=18.93. Both of them show that R increases with increasing pH.

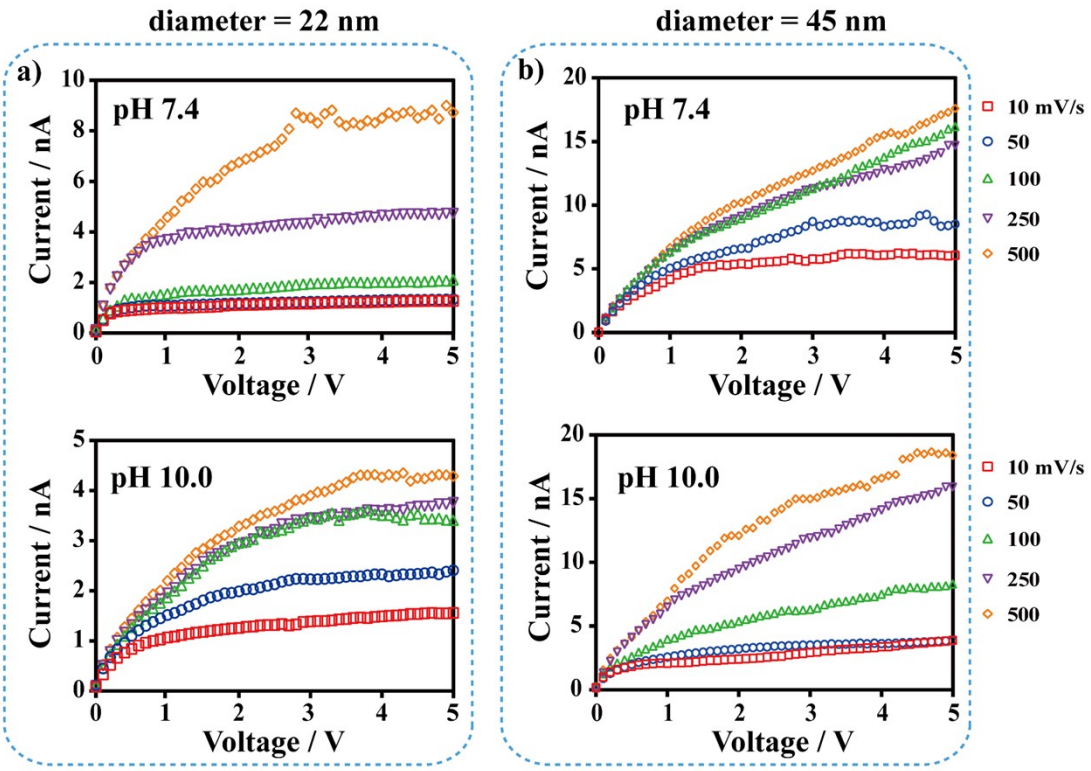

Figure S14. The partial I-V_{-5V} curves of (a) 22 nm and (b) 45nm bare quartz nanopipette in 100 mM KCl at different scan rates. □ is 10, ○ is 50, △ is 100, ▽ is 250, ◇ is 500 mV/s. There is no peak observed in I-V_{-5V}.

Finite element simulation

The COMSOL Multiphysics 5.4 software was employed for the finite element simulation. The Nernst-Plank (NP) equation is used to calculate ion mass transport, the Poisson equation provides electric potential, the Navier-Stokes (NS) equation gives the fluid motion.

The Nernst-Planck equation (Eq. 1) calculates the ion flux in the channel:

$$J_i = -D_i \nabla c_i - \frac{F z_i}{RT} D_i c_i \nabla \Phi + c_i u \quad (1)$$

where $\boldsymbol{J}_i$, D_i, c_i, z_i represent the flux, diffusion coefficient, concentration and charge of substance *i*, respectively. Φ is the local electric potential, $\boldsymbol{u}$ is the fluid velocity, F is the Faraday constant, R is the gas constant and T is the absolute temperature. The three terms on the right-hand side of Eq. 1 represent diffusive, migrative, and convective fluxes, respectively.

The ion distribution and the applied potential are linked by the Poisson equation (Eq. 2):

$$\nabla^2 \Phi = -\frac{F}{\varepsilon} \Sigma_i z_i c_i \quad (2)$$

where ε is the dielectric constant of the electrolyte and is set as 78 F/m.

The Navier-Stokes equations (Eq. 3) is used to illustrate the flow distribution:

$$u \nabla u = \frac{1}{\rho} (- \nabla p + \eta \nabla^2 u - F(\Sigma_i \sigma_i) \nabla \Phi \quad (3)$$

where ρ is the density of medium and is set to 1×10^3 kg/m^3, η is the viscosity and is set to 1×10^{-3} Pa·s, p is the pressure. Because the Reynolds number in the nanochannel is very small, the inertial terms in the Navier-Stokes equation is neglected.

The ion current of the nanochannel can be evaluated by

$$I = \int_0^r F \left(\sum_{i=1}^{N} z_i J_i \right) n \cdot 2\pi r dr \quad (4)$$

where r is the radius of nanopore, **n** is the unit normal vector.

The 2D model schematic of GP-SBA-15 is plotted in Figure S15a, and the boundary conditions are summarized in Table 1. Note that the surface charge density of DEF is

set between -0.075 and 0.01 C/m^2. We assume that the segments CDEFG are no-slip boundary conditions, while BC and HI away from the nanopore are set as a slip boundary condition.[4, 5] I-V simulation is based on time-dependent transient solution.

In addition, the 2D model schematic of nanopipette is plotted in Figure S15b, and the boundary conditions are summarized in Table 2. The aperture is set as 22 and 45 nm, the half-angle θ comes from the side-view of SEM in Figure S11b and S12b, and the surface charge density of ϕ is 0.01, 0, -0.05, -0.15, -0.25 and -0.3 C/m^2.

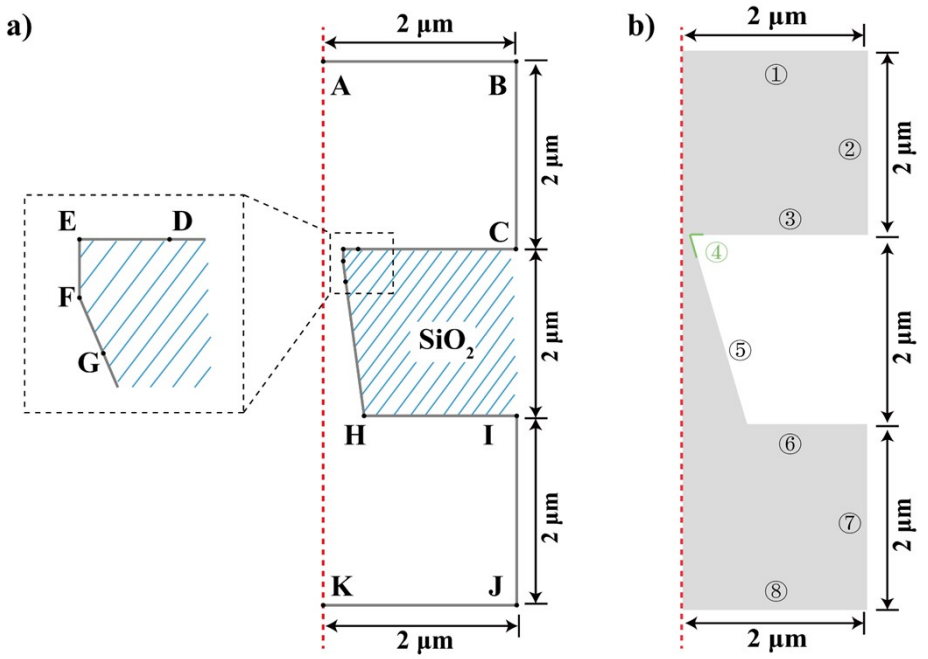

Figure S15. (a) The 2D axisymmetric simplified geometry of GP-SBA-15 for the simulation. Segments ABCDEFGHIJK show the geometric boundaries in the model. (b) The 2D axisymmetric simplified geometry of nanopipette. In (a) and (b), the red dashed line is the axis of symmetry. (c_{K^+} =0.1 M, c_{Cl^-} =0.1 M, D_{K^+} =1.957×10^{-9} m/s^2, D_{Cl^-} =2.032×10^{-9} m/s^2 at T = 298.15 K).

Table S1. Boundaries consitions of GP-SBA-15.

Segments	Nernst-Planck eq	Poisson eq	Navier-Stokes eq
AB	c_{K^+} = 0.1 M, c_{Cl^-} = 0.1 M	V = 0	p = 0
CD, GH, HI	No flux	No charge	No slip
BC, IJ	No flux	No charge	slip
DE, EF, FG	No flux	σ = 0.01, -0.025, -0.05, -0.075 C/m^2	No slip
JK	c_{K^+} = 0.1 M, c_{Cl^-} = 0.1 M	V = V	p = 0

Table S2. Boundaries consitions of nanopipette.

Segments	Nernst-Planck eq	Poisson eq	Navier-Stokes eq
1	c_{K^+} = 0.1 M, c_{Cl^-} = 0.1 M	V = 0	p = 0
3, 5, 6	No flux	No charge	No slip
2, 7	No flux	No charge	slip
4	No flux	σ = 0.01, 0, -0.05, -0.15, -0.25, -0.3 C/m^2	No slip
8	c_{K^+} = 0.1 M, c_{Cl^-} = 0.1 M	V = V	p = 0

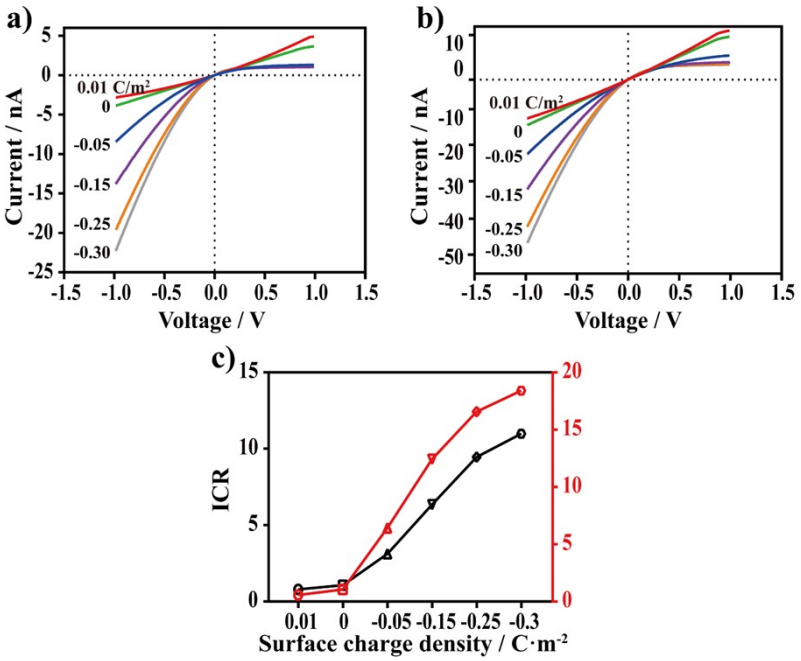

Figure S16. The simulated I-V curves of (a) 22 nm and (b) 45 nm nanopore with different surface charge densities. (c) The relationship between the ion rectification R and surface charge density calculated by FEM. Black: 45 nm, red: 22 nm. The magnitude of current and R-value are in good agreement with experiments.

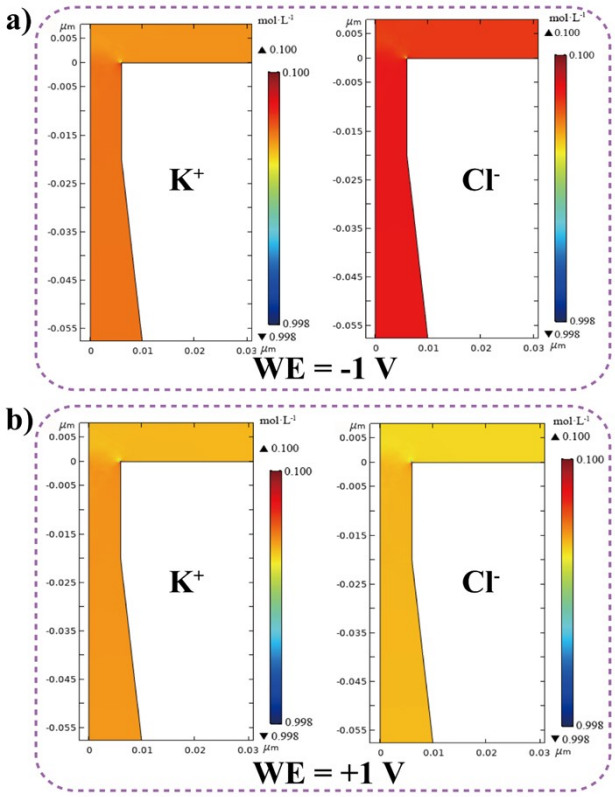

Figure S17. The ion concentration distribution of GP-SBA-15 at 0 C/m^2, (a) applied voltage is -1 V, (b) applied voltage is +1 V.

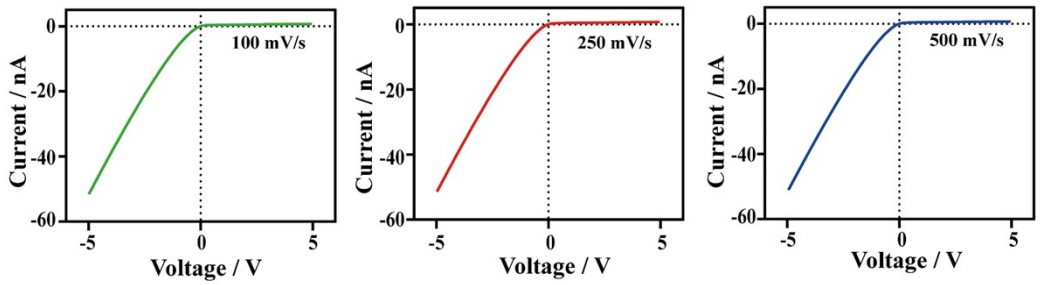

Figure S18. I-V simulations of GP-SBA-15 with different scan rate at -0.05 C/m^2 from -5 to +5 V. There is no peak calculated.

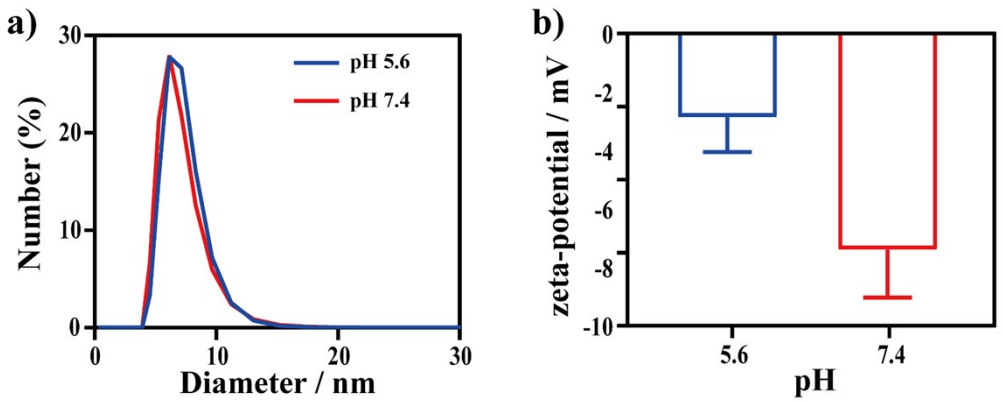

Figure S19. (a) DLS measurement and (b) zeta-potential of 1 μM BSA (10 mM PBS and 100 mM KCl) at different pH. The size and zeta-potential of BSA at pH 5.6 is (6.17±0.931) nm and (-2.29±0.952) mV, the size and zeta-potential of BSA at pH 7.4 is (7.19±1.08) nm and (-5.92±1.30) mV. The BSA is negative charged and well dispersed in the electrolyte.

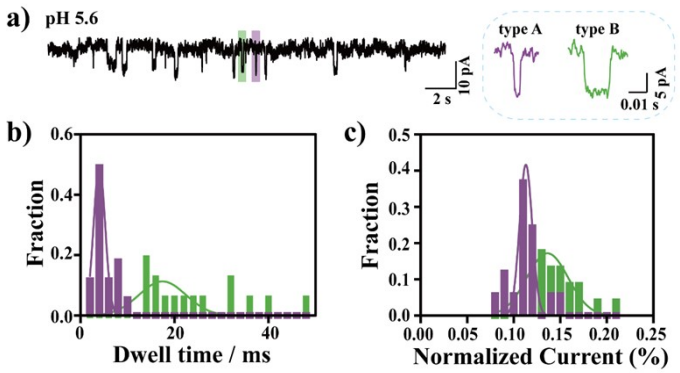

Figure S20. (a) *i-t* curve of 1 μM BSA at pH 5.6 when applied voltage is +300 mV, the representative events of type A (purple) and type B (green) are shown on the right. Gaussian distributions of type A and type B events: (b) dwell time, (c) normalized current.

References

1. Llusar, M.; Monrós, G.; Roux, C.; Pozzo, J. L.; Sanchez, C., One-pot synthesis of phenyl- and amine-functionalized silica fibers through the use of anthracenic and phenazinic organogelators. *J. Mater. Chem.* **2003,** *13*, 2505-2514.

2. Zhao, D.; Feng, J.; Huo, Q.; Melosh, N.; Fredrickson, G. H.; Chmel-ka, B. F.; Stucky, G. D., Triblock Copolymer Syntheses of Mesopo-rous Silica with Periodic 50 to 300 Angstrom Pores. *Science* **1998**, *279*, 548-552.

3. Zhao, D.; Feng, J.; Huo, Q.; Melosh, N.; Fredickson, G. H.; Chemlka, B. F.; Stucky, G. D., Triblock Copolymer Syntheses of Mesoporous Silica With Periodic 50 to 300 Angstrom Pores. *Science* **1998,** *279*, 548-552.

4. Zhang, B.; Ai, Y.; Liu, J.; Joo, S. W.; Qian, S., Polarization Effect of a Dielectric Membrane on the Ionic Current Rectification in a Conical Nanopore. *J Phys Chem C* **2011,** *115*, 24951-24959.

5. Yeh, L. H.; Zhang, M.; Qian, S., Ion transport in a pH-regulated nanopore. *Anal Chem* **2013,** *85*, 7527-34.